Available online at BCREC Website: https://bcrec.undip.ac.id

Bulletin of Chemical Reaction Engineering & Catalysis, 13 (2) 2018, 236-244

Research Article

# Electrochemical Study of Copper Ferrite as a Catalyst for $CO_2$ Photoelectrochemical Reduction

**Kaykobad Md. Rezaul Karim[1], Huei Ruey Ong[12], Hamidah Abdullah[1], Abu Yousuf[3], Chin Kui Cheng[1], Md. Maksudur Rahman Khan[1*]**

*[1]Faculty of Chemical and Natural Resources Engineering, Universiti Malaysia Pahang, Lebuhraya Tun Razak, 26300 Kuantan, Pahang, Malaysia*
*[2]Faculty of Engineering and Technology, DRB-HICOM University of Automotive Malaysia, 26607 Pekan, Pahang, Malaysia*
*[3]Faculty of Engineering Technology, Universiti Malaysia Pahang, Lebuhraya Tun Razak, 26300 Kuantan, Pahang, Malaysia*

*Received: 4th July 2017; Revised: 5th November 2017; Accepted: 15th November 2017; Available online: 11st June 2018; Published regularly: 1st August 2018*

**Abstract**

In this work, *p*-type $CuFe_2O_4$ was synthesized by sol gel method. The prepared $CuFe_2O_4$ was used as photocathode catalyst for photoelectrochemical (PEC) $CO_2$ reduction. The XRD, UV-Visible Spectroscopy (UV-Vis), and Mott-Schottky (MS) experiments were done to characterize the catalyst. Linear sweep voltammetry (LSV) was employed to evaluate the visible light ($\lambda$>400 nm) effect of this catalyst for $CO_2$ reduction. The band gap energy of the catalyst was calculated from the UV-Vis and was found 1.30 eV. Flat band potential of the prepared $CuFe_2O_4$ was also calculated and found 0.27 V versus Ag/AgCl. Under light irradiation in the $CO_2$-saturated $NaHCO_3$ solution, a remarkable current development associated with $CO_2$ reduction was found during LSV for the prepared electrode from onset potential -0.89 V with a peak current emerged at -1.01 V (vs Ag/AgCl) representing the occurrence of $CO_2$ reduction reaction. In addition, the mechanism of PEC was proposed for the photocathode where the necessity of a bias potential in the range of 0.27 to ~ -1.0 V vs Ag/AgCl was identified which could effectively inhibit the electron-hole ($e^-/h^+$) recombination process leading to an enhancement of $CO_2$ reduction reactions. 

***Keywords***: $CuFe_2O_4$; $CO_2$ reduction; onset potential; photoelectrochemical reduction; linear sweep voltammetry

***How to Cite***: Karim, K.M.R., Ong, H.R., Abdullah, H., Yousuf, A., Cheng, C.K., Khan, M.K.R. (2018). Electrochemical Study of Copper Ferrite as a Catalyst for $CO_2$ Photoelectrochemical Reduction. *Bulletin of Chemical Reaction Engineering & Catalysis*, 13 (2): 236-244 (doi:10.9767/bcrec.13.2.1317.236-244)

***Permalink/DOI***: https://doi.org/10.9767/bcrec.13.2.1317.236-244

## 1. Introduction

The rapid growth of population and industrialization leads to the generation of huge amount of $CO_2$ gas molecules through the burning of fossil fuels that causes the collapse of the natural carbon cycle and accelerates the climate change. The idea of converting $CO_2$ to hydrocarbons or oxyhydrocarbons under solar irradiation is taken from nature more specifically from plants [1-3] in which $CO_2$ and water combine to form carbohydrate over chlorophyll (catalyst) in presence of sunlight as the energy source. The mimic photosynthesis process gets huge attention in recent years giving the hopes of recycling the $CO_2$ to produce fuels that may have a large impact to solve the two major issues of present days: climate change and energy shortage [4]. Photocatalysis (PC) is one of the most promising

* Corresponding Author.
E-mail: smrkhancep@yahoo.com (M.M.R. Khan),
Telp: +6-09-5492872, Fax: +6-09-5492889

techniques to convert $CO_2$ into hydrocarbon fuels [5]. The use of photon energy in the mimic photosynthesis process requires photoresponsive materials to produce high-energy photogenerated electrons upon light irradiation [6]. To produce hydrocarbons or oxygenated hydrocarbons from $CO_2$ requires proton coupled multielectron pathways which suffer from slow reaction kinetics and poor product selectivity [7]. The single electron reduction of $CO_2$ to $\bullet CO_2^-$ occurs at -1.90 V vs normal hydrogen electrode (NHE) requiring highly reducing equivalents [8]. Proton-coupled multielectron reduction processes are used to avoid this high-energy single electron intermediate. But by this approach, it is very difficult to produce a selective product from $CO_2$ reduction [9]. The composition of the products of $CO_2$ reduction also depends on the applied potentials [10]. In this context, photocatalysis with a properly bias potential may compel the reactions to achieve required products. Moreover, the bias potential effectively reduces the $e^-/h^+$ recombination rate in the photocatalyst leading to higher quantum efficiency [11].

Metal oxide based photocatalysts have been widely investigated for $CO_2$ reduction, such as $TiO_2$ [12], $SrTiO_3$ [13], CuO-$Cu_2O$ [14], $Co_3O_4$ [10,15], $Cu_3Nb_2O_8$ [16], etc. The *p*-type metal oxides are essential for photoelectrochemical $CO_2$ reduction [5] which acted as a photocathode. In order to increase the visible light absorption efficiency, catalysts with low band gap, high electron conductivity and good stability are preferred. In recent year, $CuFe_2O_4$ has been investigated as a photocatalyst for hydrogen evolution, energy storage and decolourization [17-19]. Various methods have been used to prepare $CuFe_2O_4$, such as: hydrothermal method [20], mechanical milling [21], and sol-gel method [22]. Among those, the sol-gel method could produce high homogeneity of $CuFe_2O_4$ as well as submicron level crystallite size and higher surface to volume ratio [23]. It is well known that, $CuFe_2O_4$ possesses inverse spinel configuration with both octahedral and tetrahedral cation sites and the electron conduction is due to the electron hopping of $Fe^{2+}$ and $Fe^{3+}$ as well as $Cu^{2+}$ and $Cu^+$ sites in the spinel lattice [23,24]. In addition, it shows an excellent chemical stability in basic medium makes it very attractive to be used as catalyst [19]. Recently in our research, $CuFe_2O_4$ has been synthesized using sol-gel method and used for photocatalytic reduction of $CO_2$ where 220 $\mu mol/g_{cat}.L$ of methanol was obtained as product [25]. Due to the low band gap of $CuFe_2O_4$ it is advantageous to be used as visible light active catalyst, however the high $e^-/h^+$ recombination rate suppressed its photocatalytic efficiency [23,25]. To overcome the shortcoming, $CuFe_2O_4$ was modified by $TiO_2$ that improved the $e^-/h^+$ separation, but at the same time, this approach resulted in higher band gap of the composite material [25]. The application of bias potential in photoelectrochemical process may effectively interfere the $e^-/h^+$ recombination and can enhance the photo current leading to significant improvement in $CO_2$ reduction [11]. Based on references, there has been no information on photoelectrochemical reduction of $CO_2$ over that *p*-type $CuFe_2O_4$ in aqueous solution. In this context, the current study is focused to evaluate the photoelectrochemical characteristics of $CuFe_2O_4$ for $CO_2$ reduction. $CuFe_2O_4$ is likely to be a good photocathode due to its p-type behaviour and low band gap and the imposition of a bias potential can efficiently separate the photogenerated $e^-/h^+$ pairs accelerating the proton coupled multielectron $CO_2$ reduction. The catalyst was characterized by using UV-Vis and XRD. The photoelectrochemical behaviour of the catalyst for $CO_2$ reduction was evaluated by linear sweep voltammetry (LSV) and Mott-Schottky (MS) analysis.

## 2. Materials and Methods

### 2.1 Materials

Iron nitrate ($Fe(NO_3)_3.9H_2O$), sodium bicarbonate, ($NaHCO_3$), nitric acid ($HNO_3$, 65%), copper nitrate ($Cu(NO_3)_2.3H_2O$), isopropanol ($C_3H_8O$, 96%), nafion solution (5 wt%), and agar (acts as a gelating agent) all were in analytic condition (R&M Marketing Essex, UK). These materials were used directly without purification for this experiment. Toray carbon paper was supplied by Kuantan Sunny Scientific Collaboration Sdn. Bhd. Malaysia.

### 2.2 Catalyst preparation

$CuFe_2O_4$ was synthesized using sol-gel method with minor adjustment of reaction setting [23,26]. Copper nitrate ($Cu(NO_3)_2.3H_2O$) and ferric nitrate ($Fe(NO_3)_3.9H_2O$) with a molar ratio of 1:2 (Cu/Fe) were dissolved in 100 mL of distilled water followed by the addition of 10 mL of 65% $HNO_3$ and 16 g agar under vigorous stirring for 3 h at room temperature. Thereafter, the temperature was elevated at 90 °C and stirred continuously for another 3h. At this stage, a green gel was formed. The gel was dried at 130 °C in vacuum oven for 24 h. After that the dried powder was obtained and cal-

cined at 900 °C for 14 h. The heating rate during calcination was maintained at 10 °C/min.

### 2.3 Electrode preparation

The electrode was prepared by the method described by Woon *et al*. [27], Khan *et al*. [28], and Woon *et al*. [29]. In brief, the catalyst ink was prepared by mixing 22 mg of $CuFe_2O_4$ with 140 µL of 5 wt% nafion and 280 µL isopropanol ($C_3H_8O$) and subjected to ultra-sonication for 30 min. Thereafter, the ink was evenly brushed on the toray carbon paper with an area of 1 $cm^2$. The as prepared electrode was dried in vacuum oven at 90 °C for 6 h.

### 2.4 Catalyst characterization

The XRD results of this powdered catalyst were taken at a room temperature by means of Rigaku Mini FlexII at Bragg angle of 2θ = 10-80° with a scan rate of 0.02 °/min. During this experiment, 30 kV and 15 mA were used at Cu-Kα emission. The crystal pattern of the catalyst was assessed from the XRD results and the crystal size (D) was determined by Scherrer formula as shown in Equation 1 [30-32].

$$D = \frac{K\gamma}{B\cos\theta} \qquad (1)$$

where, $K$ is a dimensionless shape factor with a typical value of 0.9, $\lambda$ is the X-ray wave length of the applied source (0.154118 nm), and $B$ (in rad) denotes by full width of half-maximum (FWHM) of the resulting peak, determined by Gaussian fitting. UV-Visible absorption spectra of the sample were obtained by employed Shimadzu UV 2600 UV-Vis-NIR Spectrophotometer. Mott-Schottky analysis was carried out by using an electrochemical analyzer (Autolab Compact PGSTAT 204, Netherland). In this case, the prepared $CuFe_2O_4$ electrode, Ag/AgCl and platinum foil were used as working, reference and counter electrode respectively. In this case 0.1 M $NaHCO_3$ solution (pH 6.8) was used as electrolyte.

### 2.5 Photoelectrochemical analysis

The photoelectrochemical $CO_2$ reduction was carried out in a double chamber PEC cell reactor equipped with a quartz window. All the PEC measurements were done in an electrochemical work station (Autolab Compact PGSTAT 204, Netherland) using a three electrode cell consists of working electrode (prepared electrode) counter electrode (Pt-foil) and reference electrode (Ag/AgCl) in $NaHCO_3$ aqueous solution. Prior to starting the reaction, high purity $CO_2$ gas was purged for 30 min at a constant pressure until the solution reached the $CO_2$ saturation and to ensure that all dissolved $O_2$ was completely removed. Linear sweep voltammetry (LSV) was performed in between -0.6 to -1.2 V vs Ag/AgCl under the light on and dark conditions. The light on condition was maintained by using Xenon lamp (Light source: XD-300 High Brightness Cold Light Source, Beijing Perfect light Co., Ltd., China). The light was passed through the filters with different wavelengths (470, 630, and 650 nm).

## 3. Results and Discussion

### 3.1 Characterization of $CuFe_2O_4$

The XRD pattern of the $CuFe_2O_4$ is presented in Figure 1. The as-prepared $CuFe_2O_4$ can be indexed as $CuFe_2O_4$ because of similar-

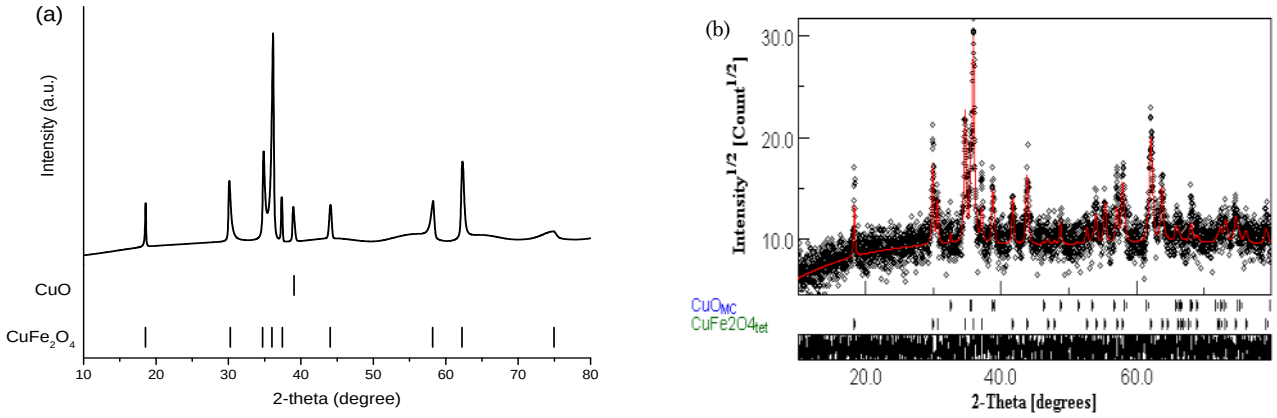


**Figure 1.** XRD results of catalyst. (a) XRD pattern of as-prepared $CuFe_2O_4$, (b) XRD pattern of as-prepared $CuFe_2O_4$ after rietveld refinement

ity with JCPDS database (peak position of 101,112, 200, 202, 211, 220, 321, 224, 400, and 422) (Figure 1a). The spectra (JCPDS 110, 200) of the sample also show the existence of trace quantity of CuO phases. According to the Scherrer principle in Equation (1), the crystal size of the $CuFe_2O_4$ is ~59 nm. To completely identify all the phases, the XRD spectra was refined with Rietveld method and presented in Figure 1b. Phase structure, microstructural parameters and lattice constants are tabulated in Table 1 as obtained from the result of Rietveld refinement with a R% of ~ 16%. Monoclinic CuO (14.67 wt %) was also found along with tetragonal $CuFe_2O_4$ (85.33 wt %). The lattice constants of $CuFe_2O_4$ and CuO are very close to the reported in the crystallographic database (ICDD 340425) and (ICDD 10706830), respectively.

The UV-Vis spectra of $CuFe_2O_4$ in the wavelength of 200-1000 nm are presented in Figure 2(a) and Tauc plot $(\alpha hv)^2$ versus band gap energy) is shown in Figure 2b to demonstrate the extrapolated intercept band gap energy value [25]. The band gap energy for as-prepared $CuFe_2O_4$ is found as 1.30 eV which is slightly lower compared to $CuFe_2O_4$ synthesized by Kezzim *et al.* [23] that reported 1.42 eV. The reduction in bandgap might be due to the increased crystallites size of $CuFe_2O_4$ (~59 nm) compared to the report of Kezzim *et al.* [23] (43 nm). The correlation of band gap with the crystallite size was presented by Marotti *et al.* [33] that revealed that the band gap could be reduced due to the increase in crystal size. Low band gap semiconductors require smaller energy to generate $e^-/h^+$ pairs which is occurred under visible light irradiation [4].

Mott-Schottky experiments were conducted in 0.1 M aqueous $NaHCO_3$ solution (pH 6.8), and the resulting plot is shown in Figure 3a. Negative slope was observed, suggesting that $CuFe_2O_4$ acted as a *p*-type semiconductor. In *p*-type semiconductors, normally, the $E_{fb}$ existed in the region of valence band (VB) which can be measured by the x-axis intercept of the plot of $1/C^2$ vs $E$ as followed by Equation (2) [16].

$$\frac{1}{C^2} = \frac{2}{e \in \in_o N}\left(E - E_{fb} - \frac{kT}{e}\right) \qquad (2)$$

where, $C$ is the capacitance, $e$ is the electron charge, $\epsilon$ is the dielectric constant, $\epsilon_0$ is permittivity of vacuum, $N$ is an acceptor density, $E$ is the electrode potential, $E_{fb}$ is the flat band potential, $k$ is the Boltzmann constant, and $T$ is the temperature. As shown in Figure 3a, the x-axis intercept was 0.25 V versus Ag/AgCl. The $E_{fb}$ was determined by using the equation $E=E_{fb}-kT/e$ and was found as 0.27 V versus Ag/AgCl. This result showed that the VB and

**Table 1.** Crystallographic parameters of as-prepared $CuFe_2O_4$ extracted from Rietveld analysis

| Sample | Phases | Composition (wt%) | symmetry | Space group | Lattice constant (Å) | | | Crystallite size (nm) | Microstrain | R% |
|---|---|---|---|---|---|---|---|---|---|---|
| | | | | | a | b | c | | | |
| $CuFe_2O_4$ | $CuFe_2O_4$ | 85.33 | Tetragonal | I41/amd:1 | 5.839 | -- | 8.656 | 59 | 15.37E-4 | 16.65 |
| | CuO | 14.67 | Monoclinic | C2/c:b1 | 4.688 | 3.425 | 5.135 | 67 | 4.02E-4 | |

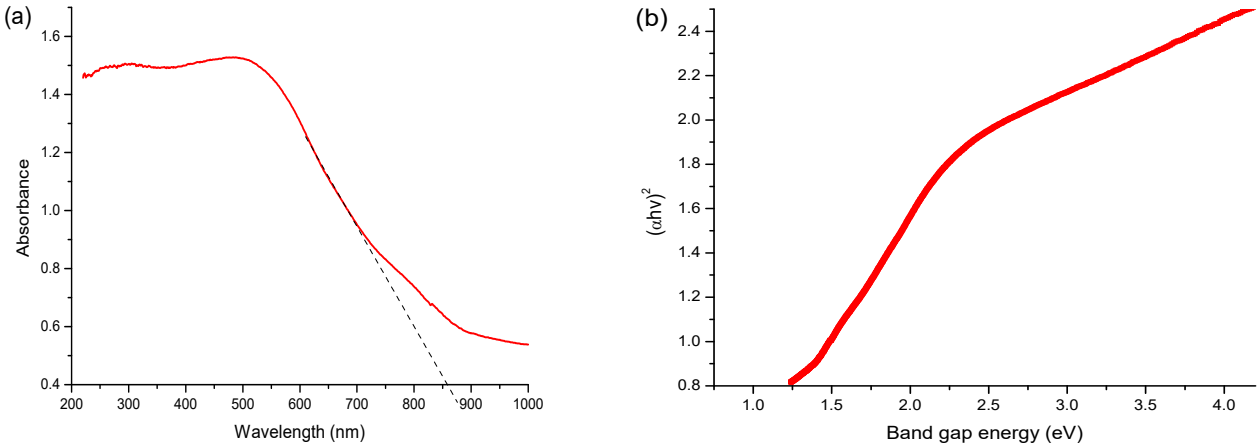


**Figure 2.** (a) UV-Vis spectra; (b) Band gap energy of $CuFe_2O_4$ photocathode catalyst

CB of *p*-type $CuFe_2O_4$ were approximately 0.27 V and -1.03 V vs Ag/AgCl, respectively. Figure 3b displays the band diagram for *p*-type $CuFe_2O_4$ and the thermodynamic redox potentials for the products of $CO_2$ reduction (V vs NHE). It can be seen that the conduction band position of the *p*-type $CuFe_2O_4$ is located in more negative position compared to the redox potentials of CO, $CH_4$, $CH_3OH$, HCOOH, and HCHO suggesting that under light irradiation the photoexcited electron from the CB of the $CuFe_2O_4$ could be transferred to $CO_2$ to occur the proton coupled multielectron $CO_2$ reduction [34,35]. In addition, a moderate bias potential in the range of 0.27 to -1.03 V vs Ag/AgCl can be applied to the system to inhibit the $e^-/h^+$ recombination to facilitate the reaction [11].

### 3.2 Photoelectrochemical activity

Figure 4 shows the voltammogram of $CuFe_2O_4$ electrode in $N_2$ and $CO_2$-saturated $NaHCO_3$ solution with and without visible light illumination. It can be seen that the shape of the voltammogram in inert condition presents similar patterns during light on and light off where the cathodic current increases with the increase of applied potential above -0.8 V which may arise from water/proton reduction [10]. In $CO_2$-saturated solution, a shoulder was observed at -1.04 V vs Ag/AgCl during light off condition, while under light irradiation a peak in cathodic current is evident at -1.01 V vs Ag/AgCl. The cathodic current further increases with the increase in applied potential beyond -1.06 V. The positive shift in the onset potential by ~70 mV under light on condition compared to the light off suggests the higher efficiency of $CO_2$ reduction under visible light irradiation.

The voltammogram in Figure 4 is in agreement with Shen *et al.* [10] and Hori *et al.* [36] that reported a similar LSV pattern in $CO_2$ saturated and inert conditions. The cathodic peak may arise due to the formation of CO intermediate from $CO_2$ [10,36]. As proposed by Schouten *et al.* [37] the cathodic current during LSV might be due to the water reduction generating proton which at higher potential may combine with adsorbed CO to form different hydrocarbons, such as methanol, methane, formaldehyde, formic acid, etc. Shen *et al.* [10] reported the production of formate as sole product during photoelectrocatalytic reduction of $CO_2$ at peak potential (-0.66 V vs NHE) over $Co_3O_4$ and Cu-$Co_3O_4$ nanotube electrodes under visible light irradiation.

Figure 5 shows the LSV voltammogram of $CuFe_2O_4$ electrode at different wavelength (470, 630, and 650 nm) along with light off in

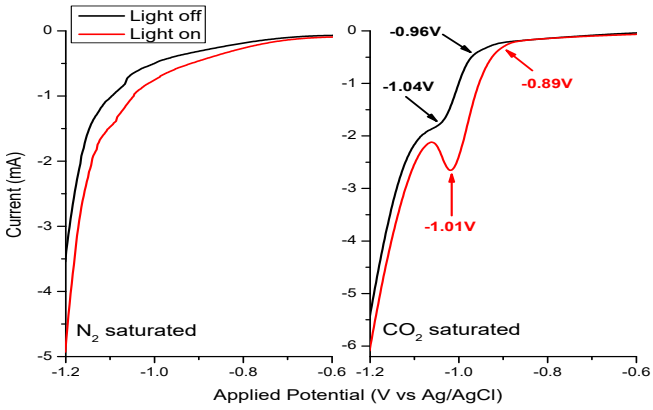


**Figure 4.** LSV of $CuFe_2O_4$ in $N_2$ and $CO_2$-saturated 0.1 M $NaHCO_3$ solution under light on/off (scan rate 10 mV/s; light wavelength = 470 nm)

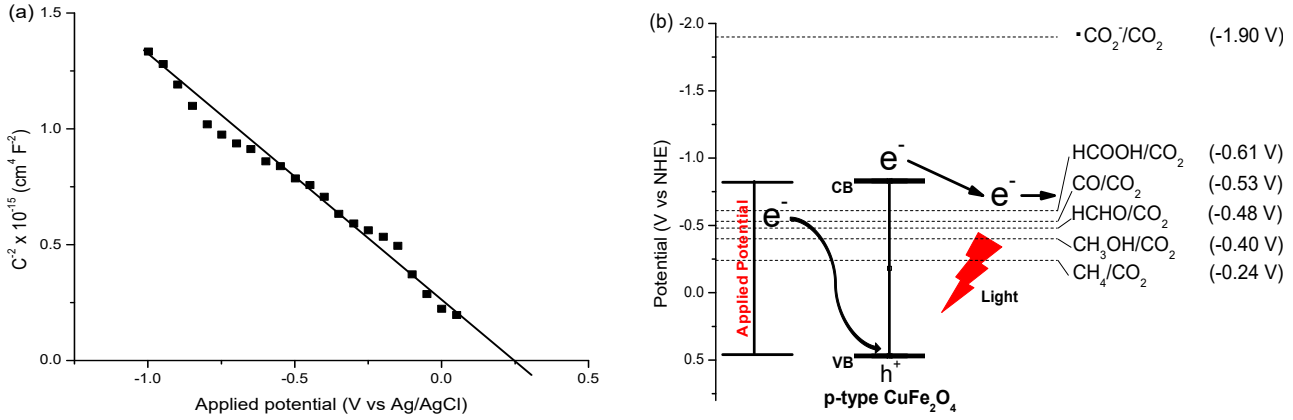


**Figure 3.** (a) Mott-schottky plot of $CuFe_2O_4$ at 2k Hz measured under light off condition; (b) Position of the CB and VB of *p*-type $CuFe_2O_4$ photocathode along with redox potential and products distribution at different potential range at pH 7

$CO_2$-saturated 0.1 M $NaHCO_3$ solution. It was found that the onset potential values were almost the same during light on conditions but shifted to more positive values compared to the light off. Furthermore, cathodic peaks were observed during light on condition at all wavelengths. When the electrode was illuminated at 470 nm wavelength the cathodic peak was shifted by 20 mV compared to the electrode illuminated at 650 nm. The result is in accordance with Figure 2a where higher visible light absorption of $CuFe_2O_4$ at 470 nm compared to 630 and 650 nm is evident.

Apart from that, concentrations of electrolyte play an important role in the reduction of $CO_2$ [38]. In Figure 6, it is found that the peak current for higher concentration of $NaHCO_3$ is significantly greater than that of lower concentration. This is due to the in higher concentration of $NaHCO_3$, more $HCO^{-3}$ ions are available to neutralize the $OH^-$ ions formed very close to catalyst surface which comes from the reduction of $H_2O$ (Equations 3-4). The pH near to the electrode surface will slightly be increased which is non-equilibrium but the overall pH of the bulk solution remains almost same (Table 2) and exist in equilibrium state [38]. As a result, the reduction of $H^+$ ions near the catalyst electrode surface are more favourable than that of bulk solution [39].

The possible reduction products of $CO_2$ were carbon monoxide, formic acid, methanol, and methane followed by $2e^-$, $4e^-$, and $8e^-$ pathway as shown in Equations 5-8:

$$2H_2O + 2e^- \rightarrow H_2 + 2OH^- \quad (3)$$
$$OH^- + HCO_3^- \rightarrow 2H_2O + CO_3^{2-} \quad (4)$$
$$CO_2 + 2H^+ + 2e^- \rightarrow CO + H_2O \quad (5)$$
$$CO_2 + 2H^+ + 2e^- \rightarrow HCOOH \quad (6)$$
$$CO_2 + 6H^+ + 6e^- \rightarrow CH_3OH + H_2O \quad (7)$$
$$CO_2 + 8H^+ + 8e^- \rightarrow CH_4 + 2H_2O \quad (8)$$

The production rate and compositions of the hydrocarbons are highly dependent on applied bias potential and catalyst materials. It is necessary to further investigate composition of the products by chromatography method and to elucidate the mechanism of the reaction. In our future work, detail study will be conducted to explore the phenomena proposed in the work.

**Table 2.** pH of $NaHCO_3$ aqueous solutions at different concentrations under $CO_2$ saturated

| [$NaHCO_3$] M | pH |
|---|---|
| 0.01 | 8.1 |
| 0.05 | 8.1 |
| 0.1 | 8.2 |
| 0.5 | 8.2 |

## 4. Conclusion

Nanostructured *p*-type $CuFe_2O_4$ was synthesized by sol-gel method. The prepared $CuFe_2O_4$ possesses a band gap of 1.3 eV with the VB and CB edges at 0.27 V and -1.03 V vs Ag/AgCl, respectively, calculated from UV-Vis and Mott-Schottky evidences. The $CuFe_2O_4$ photocathode exhibited a strong cathodic peak at -1.01 V with an onset potential of -0.89 V Ag/AgCl under the illumination of visible light. At a fixed potential (-1.01 V vs Ag/AgCl), the

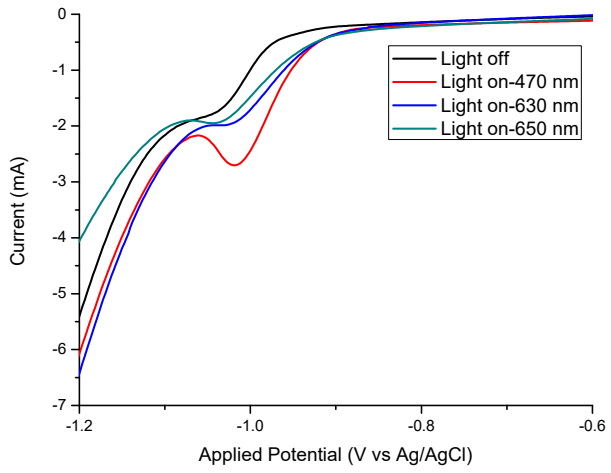


**Figure 5.** LSV of $CuFe_2O_4$ electrode in $CO_2$-saturated 0.1 M $NaHCO_3$ solution at different wavelength (scan rate 10 mV/s)

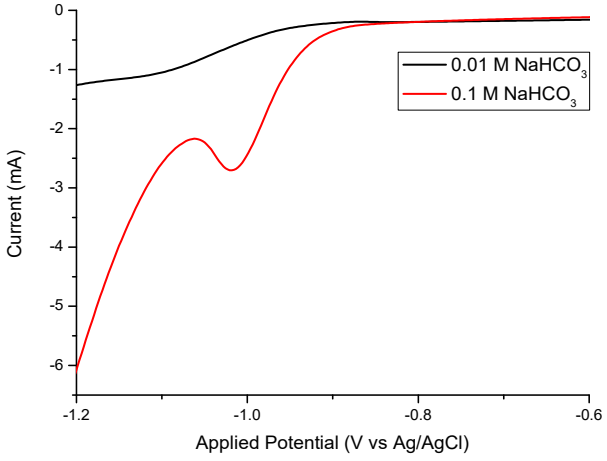


**Figure 6.** LSV of $CuFe_2O_4$ electrode in $CO_2$-saturated at different concentration of $NaHCO_3$ solution (scan rate 10 mV/s; light wavelength = 470 nm)

cathodic current increased by of 20%, 35%, and 80% at light wavelengths 650, 630, and 470 nm, respectively, compared to light off condition. The maximum light absorbance of $CuFe_2O_4$ at 470 nm is in favour of light harvesting allowing higher PEC response for $CO_2$ reduction. An electron flow scheme was proposed to demonstrate the possible mechanism for photoelectrocatalytic reduction of $CO_2$ where the proton coupled multielectron $CO_2$ reduction can produce products, such as: HCOOH, HCHO, CO, $CH_3OH$, $C_2H_4$, $C_2H_5OH$ methane, ethylene, etc. However, the identification of the products was not executed in this study. Thus, further research is required to explore the $CO_2$ reduction by PEC over *p*-type $CuFe_2O_4$ photocathode and understand the $CO_2$ reduction mechanism in depth.

## Acknowledgments

The authors would like to thank the Malaysian Ministry of Higher Education for Fundamental Research Grant Scheme (RDU 150118) and Universiti Malaysia Pahang for Postgraduate Research Grants Scheme (PGRS 170353).

## References

[1] Hu, B., Guild, C., Suib, S.L. (2013). Thermal, electrochemical, and photochemical conversion of $CO_2$ to fuels and value-added products. *Journal of $CO_2$ Utilization*, 1: 18-27.

[2] de Brito, J.F., Araujo, A.R., Rajeshwar, K., Zanoni, M.V.B. (2015). Photoelectrochemical reduction of $CO_2$ on $Cu/Cu_2O$ films: Product distribution and pH effects. *Chemical Engineering Journal*, 264: 302-309.

[3] Jhong, H.-R.M., Ma, S., Kenis, P.J.A. (2013). Electrochemical conversion of $CO_2$ to useful chemicals: current status, remaining challenges, and future opportunities. *Current Opinion in Chemical Engineering*, 2: 191-199.

[4] Jiang, Z., Xiao, T., Kuznetsov, V., Edwards, P., Turning carbon dioxide into fuel, 2010.

[5] Awad, N.K., Ashour, E.A., Allam, N.K. (2014). Recent advances in the use of metal oxide-based photocathodes for solar fuel production. *Journal of Renewable and Sustainable Energy*, 6: 022702.

[6] Abdullah, H., Khan, M.M.R., Ong, H.R., Yaakob, Z. (2017). Modified $TiO_2$ photocatalyst for $CO_2$ photocatalytic reduction: An overview. *Journal of $CO_2$ Utilization*, 22: 15-32.

[7] Tu, W., Zhou, Y., Zou, Z. (2014). Photocatalytic Conversion of $CO_2$ into Renewable Hydrocarbon Fuels: State-of-the-Art Accomplishment, Challenges, and Prospects. *Advanced Materials*, 26: 4607-4626.

[8] Schwarz, H.A., Dodson, R.W. (1989). Reduction potentials of $CO_2$- and the alcohol radicals. *Journal of Physical Chemistry*, 93.

[9] Qiao, J., Liu, Y., Hong, F., Zhang, J. (2014). A review of catalysts for the electroreduction of carbon dioxide to produce low-carbon fuels. *Chemical Society Reviews*, 43: 631-675.

[10] Shen, Q., Chen, Z., Huang, X., Liu, M., Zhao, G. (2015). High-yield and selective photoelectrocatalytic reduction of $CO_2$ to formate by metallic copper decorated $Co_3O_4$ nanotube arrays. *Environmental science & technology*, 49: 5828-5835.

[11] Pesci, F.M., Wang, G., Klug, D.R., Li, Y., Cowan, A.J. (2013). Efficient Suppression of Electron–Hole Recombination in Oxygen-Deficient Hydrogen-Treated $TiO_2$ Nanowires for Photoelectrochemical Water Splitting. *The Journal of Physical Chemistry C*, 117: 25837-25844.

[12] Sierra-Ávila, R., Pérez-Alvarez, M., Cadenas-Pliego, G., Ávila-Orta, C.A., Betancourt-Galindo, R., Jiménez-Regalado, E., Jiménez-Barrera, R.M., Martínez-Colunga, J.G. (2014). Synthesis of Copper Nanoparticles Coated with Nitrogen Ligands. *Journal of Nanomaterials*, 2014: 361791.

[13] Shoji, S., Yin, G., Nishikawa, M., Atarashi, D., Sakai, E., Miyauchi, M. (2016). Photocatalytic reduction of $CO_2$ by CuxO nanocluster loaded $SrTiO_3$ nanorod thin film. *Chemical Physics Letters*, 658: 309-314.

[14] Ghadimkhani, G., de Tacconi, N.R., Chanmanee, W., Janaky, C., Rajeshwar, K. (2013). Efficient solar photoelectrosynthesis of methanol from carbon dioxide using hybrid $CuO-Cu_2O$ semiconductor nanorod arrays. *Chemical Communications*, 49: 1297-1299.

[15] Huang, X., Cao, T., Liu, M., Zhao, G. (2013). Synergistic photoelectrochemical synthesis of formate from $CO_2$ on {121} hierarchical $Co_3O_4$. *The Journal of Physical Chemistry C*, 117: 26432-26440.

[16] Kamimura, S., Murakami, N., Tsubota, T., Ohno, T. (2015). Fabrication and characterization of a p-type $Cu_3Nb_2O_8$ photocathode toward photoelectrochemical reduction of carbon dioxide. *Applied Catalysis B: Environmental*, 174: 471-476.

[17] Yang, H., Yan, J., Lu, Z., Cheng, X., Tang, Y. (2009). Photocatalytic activity evaluation of tetragonal $CuFe_2O_4$ nanoparticles for the $H_2$ evolution under visible light irradiation. *Journal of Alloys and Compounds*, 476: 715-719.

[18] Fu, Y., Chen, Q., He, M., Wan, Y., Sun, X., Xia, H., Wang, X. (2012). Copper ferrite-graphene hybrid: a multifunctional heteroarchitecture for photocatalysis and energy stor-

age. *Industrial & Engineering Chemistry Research*, 51: 11700-11709.

[19] Zhao, Y., He, G., Dai, W., Chen, H. (2014). High catalytic activity in the phenol hydroxylation of magnetically separable $CuFe_2O_4$-reduced graphene oxide. *Industrial & Engineering Chemistry Research*, 53: 12566-12574.

[20] Nakhjavan, B., Tahir, M., Panthöfer, M., Gao, H., D. Schladt, T., Gasi, T., Ksenofontov, V., Branscheid, R., Weber, S., Kolb, U., Schreiber, L., Tremel, W., Synthesis, characterization and functionalization of nearly monodisperse copper ferrite $Cu_{(x)}Fe_{(3-x)}O_{(4)}$ nanoparticles, *Journal of Materials Chemistry*, 21: 6909-6915

[21] Goya, G.F. (1997). Nanocrystalline $CuFe_2O_4$ obtained by mechanical grinding. *Journal of Materials Science Letters*, 16: 563-565.

[22] Valdés-Solís, T., Tartaj, P., Marbán, G., Fuertes, A.B. (2007). Facile synthetic route to nanosized ferrites by using mesoporous silica as a hard template, *Nanotechnology*, 18: 145603

[23] Kezzim, A., Nasrallah, N., Abdi, A., Trari, M. (2011). Visible light induced hydrogen on the novel hetero-system $CuFe_2O_4/TiO_2$. *Energy Conversion and Management*, 52: 2800-2806.

[24] Selvan, R.K., Augustin, C.O., Šepelák, V., Berchmans, L.J., Sanjeeviraja, C., Gedanken, A. (2008). Synthesis and characterization of $CuFe_2O_4/CeO_2$ nanocomposites. *Materials Chemistry and Physics*, 112: 373-380.

[25] Uddin, M.R., Khan, M.R., Rahman, M.W., Yousuf, A., Cheng, C.K. (2015). Photocatalytic reduction of $CO_2$ into methanol over $CuFe_2O_4/TiO_2$ under visible light irradiation. *Reaction Kinetics, Mechanisms and Catalysis*, 116: 589-604.

[26] Khan, M.M.R., Uddin, M.R., Abdullah, H., Karim, K.M.R., Yousuf, A., Cheng, C.K., Ong, H.R. (2016). Preparation and Characterization of $CuFe_2O_4/TiO_2$ Photocatalyst for the Conversion of $CO_2$ into Methanol under Visible Light. *International Journal of Chemical, Molecular, Nuclear, Materials and Metallurgical Engineering*, 10: 1165-1172.

[27] Woon, C.W., Ong, H.R., Chong, K.F., Chan, K.M., Khan, M.M.R. (2015). $MnO_2$/CNT as ORR Electrocatalyst in Air-Cathode Microbial Fuel Cells. *Procedia Chemistry*, 16: 640-647.

[28] Khan, M.R., Chan, K.M., Ong, H.R., Cheng, C.K., Rahman, W. (2015). Nanostructured Pt/$MnO_2$ Catalysts and Their Performance for Oxygen Reduction Reaction in Air Cathode Microbial Fuel Cell. *International Journal of Electrical, Computer, Electronics and Communication Engineering*, 9: 247-253.

[29] Woon, C.W., Islam, M.A., Ethiraj, B., Ong, H.R., Cheng, C.K., Chong, K.F., Hedge, G., Khan, M., Rahman, M. (2017). Carbon Nanotube-Modified $MnO_2$: An Efficient Electrocatalyst for Oxygen Reduction Reaction. *Chemistry Select.*, 2: 7637-7644.

[30] Prasad, D.M.R., Rahmat, N.S.B., Ong, H.R., Cheng, C.K., Khan, M.R., Sathiyamoorthy, D. (2016). Preparation and Characterization of Photocatalyst for the Conversion of Carbon Dioxide to Methanol. *International Journal of Chemical, Molecular, Nuclear, Materials and Metallurgical Engineering*, 10: 464-467.

[31] Mandal, D., Sharma, L.K., Mukherjee, S. (2016). Defect-induced weak ferromagnetism in transition metal-doped ZnO nanoparticles. *Applied Physics A*, 122: 1033.

[32] Akhtar, M.S., Riaz, S., Mehmood, R.F., Ahmad, K.S., Alghamdi, Y., Malik, M.A., Naseem, S. (2017). Surfactant and template free synthesis of porous ZnS nanoparticles. *Materials Chemistry and Physics*, 189: 28-34.

[33] Marotti, R.E., Giorgi, P., Machado, G., Dalchiele, E.A. (2006). Crystallite size dependence of band gap energy for electrodeposited ZnO grown at different temperatures. *Solar Energy Materials and Solar Cells*, 90: 2356-2361.

[34] Wang, J.-C., Zhang, L., Fang, W.-X., Ren, J., Li, Y.-Y., Yao, H.-C., Wang, J.-S., Li, Z.-J. (2015). Enhanced Photoreduction $CO_2$ Activity over Direct Z-Scheme α-$Fe_2O_3/Cu_2O$ Heterostructures under Visible Light Irradiation. *ACS Appl. Mater. Interfaces*, 7: 8631-8639.

[35] Zhu, X., Yang, D., Wei, W., Jiang, M., Li, L., Zhu, X., You, J., Wang, H. (2014). Magnetic copper ferrite nanoparticles/TEMPO catalyzed selective oxidation of activated alcohols to aldehydes under ligand- and base-free conditions in water. *RSC Advances*, 4: 64930-64935.

[36] Hori, Y., Murata, A., Takahashi, R. (1989). Formation of hydrocarbons in the electrochemical reduction of carbon dioxide at a copper electrode in aqueous solution. *Journal of the Chemical Society, Faraday Transactions 1: Physical Chemistry in Condensed Phases*, 85: 2309-2326.

[37] Schouten, K.J.P., Kwon, Y., van der Ham, C.J.M., Qin, Z., Koper, M.T.M. (2011). A new mechanism for the selectivity to $C_1$ and $C_2$ species in the electrochemical reduction of carbon dioxide on copper electrodes. *Chemical Science*, 2: 1902-1909.

[38] Hori, Y., Murata, A., Takahashi, R., Suzuki, S. (1988). Enhanced formation of ethylene and alcohols at ambient temperature and pressure in electrochemical reduction of carbon dioxide at a copper electrode. *Journal of the Chemical Society, Chemical Communications*, 1: 17-19.

[39] Gu, J., Wuttig, A., Krizan, J.W., Hu, Y., Detweiler, Z.M., Cava, R.J., Bocarsly, A.B. (2013). Mg-Doped $CuFeO_2$ photocathodes for photoelectrochemical reduction of carbon dioxide. *The Journal of Physical Chemistry C*, 117: 12415-12422.